Eur Biophys J (1996) 25: 93–103

ARTICLE

Andreas Janshoff · Joachim Wegener · Manfred Sieber
Hans-Joachim Galla

Double-mode impedance analysis of epithelial cell monolayers cultured on shear wave resonators

Received: 5 June 1996 / Accepted: 6 August 1996

Abstract The viscoelastic behavior of epithelial cells (MDCK-I and MDCK-II) grown on AT-cut quartz crystals with a fundamental resonance at 5 MHz was investigated by impedance spectroscopy. Using the electromechanical model recently derived by Martin et al. [(1991) Anal Chem 63: 2272–2281] for Newtonian liquids in contact with shear wave resonators we quantified the viscous damping arising from the adherent cells by fitting the impedance data with a modified Butterworth-Van Dyke circuit in the region of the resonance frequency. Impedance spectroscopy was additionally performed in the frequency range from 1 Hz to 1 MHz to scrutinize the passive electrical properties of the epithelial cell layers using an additional platinum electrode. These data allow one to document the cell layers' integrity as well as the electrode coverage. We were able to confirm that the presence of a cell-layer mainly increases damping of the shear wave and does not exhibit a pure mass-load behavior. These findings were supported by the discovery that the inductance L in the electromechanical model was less influenced by the cell-layer than the resistance R. The apparent cell-viscosities determined by our method are 0.097 poise for MDCK-I and 0.142 poise for MDCK-II cell-layers. These low apparent viscosities may be explained in terms of a considerable spacing between the cells immobilized via their focal contacts and the quartz surface.

Key words Impedance analysis · MDCK-cells · Quartz crystal microbalance (QCM)

Abbreviations QCM quartz crystal microbalance · MDCK Madin-Darby Canine-Kidney · EDTA ethylene diamine tetraacetate · TER transepithelial electrical resistance · SDM standard deviation mean

A. Janshoff · J. Wegener · M. Sieber · H.-J. Galla (✉)
Institute of Biochemistry, Westfälische Wilhelms-University, Wilhelm-Klemm-Strasse 2, D-48149 Münster, Germany
(Fax: +49 251 833206; e-mail: Hajo.Galla @uni-muenster.de)

1. Introduction

The quartz crystal microbalance (QCM) has been widely accepted as a microgravimetric sensor for deposition processes in the gas phase. According to Sauerbrey, mass loading onto a quartz surface causes a proportional shift in the resonance frequency of the shear resonator (Sauerbrey 1959). The development of quartz crystal units operating under liquid loading – especially with one side of the crystal under water – has opened a variety of different applications in sensor technology, such as deposition monitoring of adsorption processes in electrochemistry (Xu and Schlenoff 1995; Schneider and Buttry 1993) and biosensor devices based on immunoassays (Muramatsu et al. 1987). Most of the previous studies made use of the so called 'active oscillator method' in which the quartz resonator is part of an oscillator circuit equipped with high gain amplifier units necessary to cope with the increased damping due to the viscous coupling of the liquid. The main disadvantage of this method is its limitation to one single parameter that may be recorded, the resonant frequency. Therefore, the various different properties of a particular system that influence the shear vibration of a quartz resonator may not be resolved. While in most studies dealing with shear resonators as biosensor devices the change in the resonance frequency is directly related to rigid mass loading based on Sauerbrey's equation, this assumption could be too simplified as the frequency change could be a combined effect of viscous coupling of the adsorbed species and its mass loading. In this context the pioneering work of Kanazawa and Gordon (1985), Muramatsu et al. (1988), Reed et al. (1990) and Glassford (1978) should be emphazised because of their first approaches taking viscous damping into account. In an elegant study Yang and Thompson (1993) (see also Kippling and Thompson 1990) showed that network analysis of the loaded quartz crystal provides multiple chemical information about the liquid in contact with the quartz surface. These findings are based on a theoretical model established by Martin et al. (1991) who derived an equivalent circuit representing bulk acous-

tic shear resonators that operate under simultaneous liquid and mass loading. Following Martin's theory, impedance analysis in the frequency range close to the resonance frequencies of the quartz crystal easily solves the problem of distinguishing between rigid mass loading arising for example from electrodeposition of metals and the viscous coupling of liquids.

As the quartz resonator has proven to be very sensitive to the viscous properties of the contacting liquid we used impedance analysis to study epithelial cell monolayers cultured on the quartz surface. In contrast to other groups (Redepenning et al. 1993; Ebato et al. 1993; Gryte et al. 1993) who successfully cultured different cell types on top of shear resonators and recorded cell-growth by using the active oscillater method, this study is intended to clarify the influence of epithelial cell monolayers on the shear vibration of a quartz resonator in detail using impedance analysis and subsequent equivalent circuit modelling.

In order to demonstrate the presence of a confluent cell monolayer on top of the quartz resonator and its intactness over the entire active surface, we made use of epithelial barrier properties. The predominant physiological function of epithelial cell layers is to build up and maintain a highly selective permeability barrier between two fluid compartments, intended to avoid free diffusion of hydrophilic solutes and ions from one compartment to the adjacent one. One physical parameter to quantify the barrier function of a given epithelial cell layer – as far as ion permeation is concerned – is the electrical resistance across this cell layer, which is commonly called the transepithelial electrical resistance (TER). Recently we introduced a new method, based on impedance spectroscopy, that enables one to determine TERs of cell monolayers cultured on gold surfaces (Wegener et al. 1996). As an effective epithelial barrier requires an entirely confluent cell monolayer with intact cell-cell-contacts, impedance analysis of the epithelial cell layer allows one to document surface coverage of the quartz resonator in situ.

We chose to combine our experimental setup to measure TERs with the quartz crystal microbalance technique (QCM) in order to determine both the electrical and the viscoelastic properties of an MDCK epithelial cell-monolayer in one measurement.

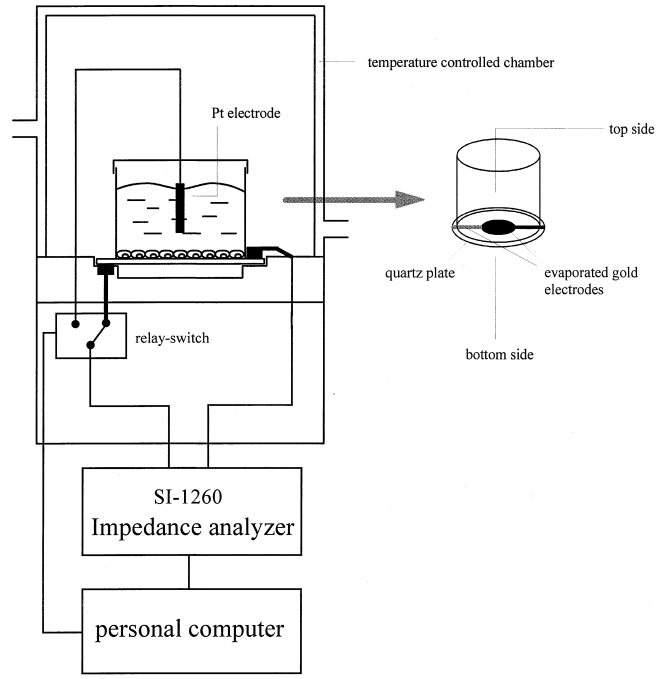

Fig. 1 Experimental setup used in this study consisting of a temperature controlled quartz crystal holder connected via a relay switch to a SI 1260 gain/phase impedance analyzer. The electrode on the bottom side of the quartz resonator was placed on a copper ring while the electrode on top of the quartz plate is contacted via modified relay contacts. The relay allows one to switch between the electrodes in order to perform either *cell mode* or *quartz mode* experiments. The impedance analyzer as well as the relay are controlled by a personal computer. The *quartz mode* measurements are performed in the frequency range from 4.97 to 5.04 MHz whereas the *cell mode* is recorded in the range of $1-10^6$ Hz

2. Materials and methods

2.1 Measuring device

The experimental setup used in the present study is schematically depicted in Fig. 1. It basically consists of the quartz resonator, a temperature controlled quartz crystal holder and an additional platinum electrode necessary to perform impedance analysis of the epithelial cell layer. In detail, we used a non-cytotoxic silicon glue (Elchsiegel, Rhône Poulenc, Germany) to fix small glass tubes (d = 10 mm) onto overtone polished AT-cut (plano-plano) 5 MHz quartz resonators (KVG, Niederbischofsheim, Germany) (d = 14 mm) in order to form a culture dish like container providing only small mounting losses. The quartz resonators are covered with evaporated gold electrodes (d = 6 mm) on both sides of the quartz plate. This culture dish may be closed by a screw cap to avoid evaporation of water and bacterial contamination. The screw cap furthermore serves to mechanically fix the platinized platinum electrode that is immersed in the bulk electrolyte as illustrated in Fig. 1.

The quartz dish was mounted into the crystal holder consisting of modified gold-relay contacts touching the upper side and a small copper-ring connecting the bottom side of the quartz plate. A computer controlled relay allows one to connect either the two gold electrodes on opposite sides of the quartz plate (*quartz mode*) or the gold electrode facing the liquid together with the platinum electrode (*cell mode*) to the continuous wave impedance analyzer (Solartron Instruments, SI 1260) via very short shielded cables.

Impedance analysis in the *quartz mode* was carried out in the frequency range from 4.97 to 5.04 MHz using a sinusoidal a.c. voltage of 150 mV amplitude. Within the given frequency range 500 data points were recorded. The passive electrical properties of the cell layers (*cell mode*)

were determined using an a. c. voltage of 10 mV amplitude in the frequency range from 1 Hz to 1 MHz reading a total of 70 data points that were chosen to be equidistant on a logarithmic scale.

Quantitative analysis of the impedance spectra obtained in either mode was achieved by fitting the parameters of appropriate equivalent circuits, representing the electrical properties of the particular system under investigation, to the recorded data by means of a non-linear-least-square-fit according to the Levenberg-Marquardt-algorithm. In the case of *cell mode* spectra we used a weighted fit in which the weighting factors were assumed to be proportional to the measured value. Phase spectra as recorded in *quartz mode* measurements were analyzed unweighted. Fitting routines were performed using self-developed software.

2.2 Cell culture

The present study was intended to investigate cell monolayers formed by cells of either strain I or II of the epithelial cell line MDCK (Madin-Darby Canine Kidney), abbreviated MDCK-I and MDCK-II. Both strains of MDCK cells were cultured identically. We used MEM-Earle (Seromed) as culture medium additionally supplemented with 4 mM L-glutamine (Seromed), 100 mg/l penicillin (Seromed), 100 mg/l streptomycin (Seromed) and 10% (v/v) fetal calf serum (PAA). Stocks of both cell types were grown in a humidified incubator (Heraeus) with a 5% CO_2 and 95% air atmosphere.

Prior to any QCM-experiment the whole quartz dish was sterilized by an argon plasma (Harrick) treatment for three to five minutes. Cells were removed from the ordinary tissue flask by trypsin digestion [0.25% (w/v) trypsin and 1 mM EDTA in phosphate buffered saline] and seeded into the quartz dish without any precoating of the quartz plate. The quartz dish stayed in the incubator until a confluent cell layer was established. Confluent monolayers were investigated at room temperature (23 °C). To determine the properties of the uncovered quartz plate in the QCM-experiment cells were removed from the quartz surface using a rubber policeman.

In order to estimate the average density of both cell types, freshly trypsinated cells were resuspended in culture medium and the suspension was split equally. Aliquots were carefully transferred onto seven different Percoll® solutions with incresaing density [1.03 g/cm^3 to 1.07 g/cm^3]. The whole system was exposed to a 690 *g* centrifugation at 23 °C for 10 min. The average density of each cell strain was estimated from the localization of cells after the centrifugation procedure, either at the culture medium/Percoll interface, within the Percoll-solution or by the formation of a pellet. Cellular density was considered to be equal to the density of that particular Percoll-solution, in which most of the cells were localized within the Percoll-solution but neither at the interface nor in the pellet. Densities of the Percoll-solutions were determined using a Gay-Lussac pycnometer.

2.3 Confirmation of surface coverage

As the optical qualities of the quartz plates together with the evaporated gold electrodes on opposite sides of the quartz do not allow one to document cell growth onto the quartz surface by common phase contrast microscopy, we chose an indirect approach to confirm the presence of a confluent epithelial cell layer on top of the active quartz surface. We made use of special impedance measurement chambers that are suitable for performing *cell mode* analogue measurements together with optical observations of the cultured cells that have been described in detail elsewhere (Wegener et al. 1996). These chambers briefly consist of ordinary microscope slides covered with evaporated gold films that serve as measuring electrodes. These gold electrodes were prepared thin enough to be transparent, so that cell growth on top of these gold electrodes may be documented by ordinary light microscopes. The whole setup is completed by a glass top that allows one to use these impedance measurement chambers like ordinary cell culture dishes with a very similar architecture compared to the quartz dishes used in the present study. MDCK-II cells were seeded into these impedance measurement chambers immediately after trypsin mediated removal from the culture flask and then surface coverage of the gold electrodes was documented by aquisition of *cell mode* impedance spectra together with phase contrast micrographs. Figure 4 depicts phase contrast micrographs of four different culture stages together with the corresponding *cell mode* impedance spectra.

2.4 Calibration measurements with glycerol/water mixtures of known density and viscosity

In order to quantify the apparent viscosity of the cell monolayers under investigation we chose to calibrate our experimental setup with glycerol/water mixtures of known density and viscosity (Weast 1982). This set of glycerol/water-mixtures was investigated by *quartz mode* measurements at 23 °C.

3. Results

3.1 Cell mode measurements

Two different strains of the epithelial cell line MDCK were investigated using impedance spectroscopy in the *quartz* and in the *cell mode.* Both strains are very popular *in vitro* systems to elucidate the special characteristics of a transporting epithelium in tissue culture. They are very similar with respect to their morphological characteristics but differ in their ability to build high resistant barriers to the permeation of ions as expressed in their specific TERs. Whereas MDCK-II cells exhibit TERs in the range of 100 to 300 $\Omega \cdot cm^2$ and are regarded as belonging to the leaky epithelia, MDCK-I cell layers characteristically show TER

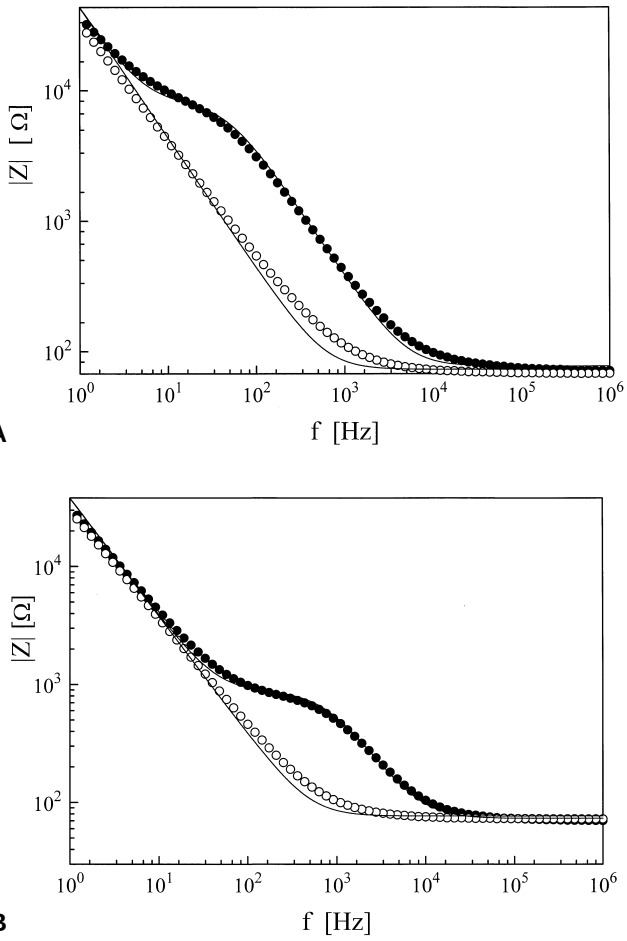

Fig. 2 A, B Typical *cell mode* impedance spectra [|Z|(f)] before (●) and after (○) removal of confluent MDCK cell monolayers. The outcome of the non-linear least square fit according to the equivalent circuit given in Fig. 3 A is depicted as a *solid line*. **A** MDCK-I: $R_{c.l.} = 1926\ \Omega \cdot cm^2$; $C_{c.l.} = 1.8\ \mu F/cm^2$; **B** MDCK-II: $R_{c.l.} = 203\ \Omega\ cm^2$; $C_{c.l.} = 1.1\ \mu F/cm^2$

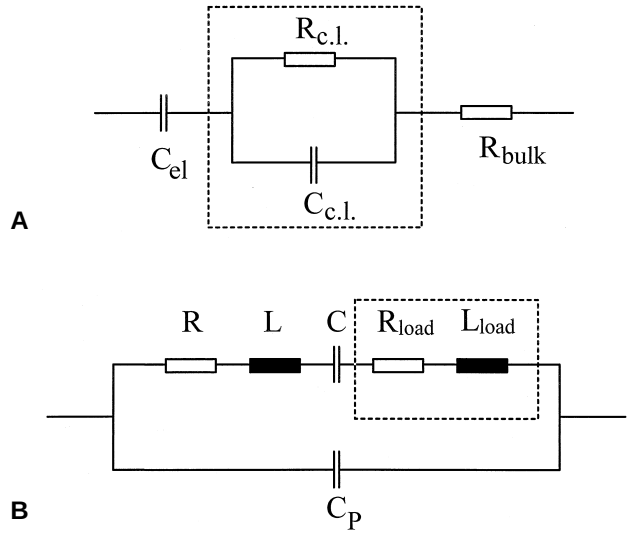

Fig. 3 A presents the equivalent circuit used for curve fitting of *cell-mode* experiments. Again the dotted box represents the influence of the cell monolayer on the impedance spectra. $R_{c.l.}$ represents the transepithelial resistance arising form the formation of tight-junctions between the cells, $C_{c.l.}$ is the capacitance of the cell-monolayer. A detailed explanation is given in the text. B shows the equivalent circuit used for nonlinear fitting of the phase spectra recorded in *quartz-mode* measurements. R, L, C and C_P are the parameters of the unperturbed quartz crystal while the additional elements R_{load} and L_{load} represent the liquid loading and the cell monolayer, respectively, attached to the quartz surface

values of 1 to 5 $k\Omega \cdot cm^2$ and are therefore classified as a tight epithelium.

In a recent paper (Wegener et al. 1996) we presented a rather new technique to determine TERs of epithelial and endothelial cell monolayers that were cultured onto gold surfaces. For the present study we modified this technique from using a coplanar arrangement of two gold electrodes to the use of Au/Pt electrodes in a sandwich arrangement with respect to the cell layer (Fig. 1), which has proven not to influence the outcome of the determination procedure. Typical impedance spectra as they were recorded in the *cell mode* for MDCK-I and MDCK-II cells are depicted in Fig. 2 A and 2 B together with the impedance spectra of the uncovered gold electrodes. The presence of the epithelial cell layers on top of the gold electrodes obviously alters the frequency dependent impedance of the particular system in the frequency range from 100 Hz to 10 kHz. For a quantitative analysis of these impedance spectra we used the equivalent circuit shown in Fig. 3 A. The outcome of the fitting procedure is depicted as solid lines within Fig. 2 A and 2 B. The impedance elements of the equivalent circuit may be subdivided into cell-related elements (dotted box) and not-cell-related elements: C_{el} represents the dielectric properties of the electrode/electrolyte interface, R_{bulk} represents the ohmic resistance of the bulk electrolyte, $R_{c.l.}$ is interpreted as the transepithelial electrical resistance whereas $C_{c.l.}$ represents the cell layer's capacitance. The illustrated circuit is the simplest model to fully describe the characteristics of the obtained spectra using a minimum number of parameters. Deviations between our model and the experimental data in a frequency range below 1 kHz may be attributed to the simplified treatment of the electrode/electrolyte interface as an ideal capacitor in series with an ohmic resistor for the conductivity of the bulk, which is strictly correct only for liquid mercury electrodes with perfectly smooth surfaces (McAdams 1995). Owing to the unspecific adsorption of medium ingredients to the electrode surface together with the non ideal surface topography of solid metal electrodes, this is of course a simplified assumption but does not interfere with the outcome of our experiments.

Therefore *cell mode* measurements provide two independent parameters to describe the passive electrical properties of the cell monolayers. Transepithelial resistances and cellular capacitances as they were determined for MDCK-I and MDCK-II cells cultured on top of quartz resonators are summarized in Table 1. They were found to

Table 1 Mean values for the parameters R_{total}, ΔR_{total} and ΔL_{total} as deduced from *quartz mode* measurements and subsequent equivalent circuit modelling together with the corresponding mean values for the parameters $R_{c.l.}$ and $C_{c.l.}$ as derived from *cell mode* data. The statistical evaluation covers a total of 8 MDCK-I and 7 MDCK-II quartzes. All data are given as mean±SDM. R_{total} represents the motional resistance as derived from impedance analysis of the cell covered shear wave resonator, ΔR_{total} and ΔL_{total} reflect the differences in motional resistances and inductances, respectively, before and after cell removal. $R_{c.l.}$ and $C_{c.l.}$ represent the passive electrical properties of the cell monolayers

	R_{total} [Ω]	ΔR_{total} [Ω]	ΔL_{total} [μH]	$R_{c.l.}$ [Ω · cm^2]	$C_{c.l.}$ [μF/cm^2]
MDCK I	1444 ± 28	755 ± 36	6.7 ± 0.7	1543 ± 252	1.46 ± 0.06
After cell removal	690 ± 8	–	–		
MDCK II	1673 ± 22	992 ± 36	10.5 ± 0.8	206 ± 11	1.09 ± 0.02
After cell removal	681 ± 14	–	–		

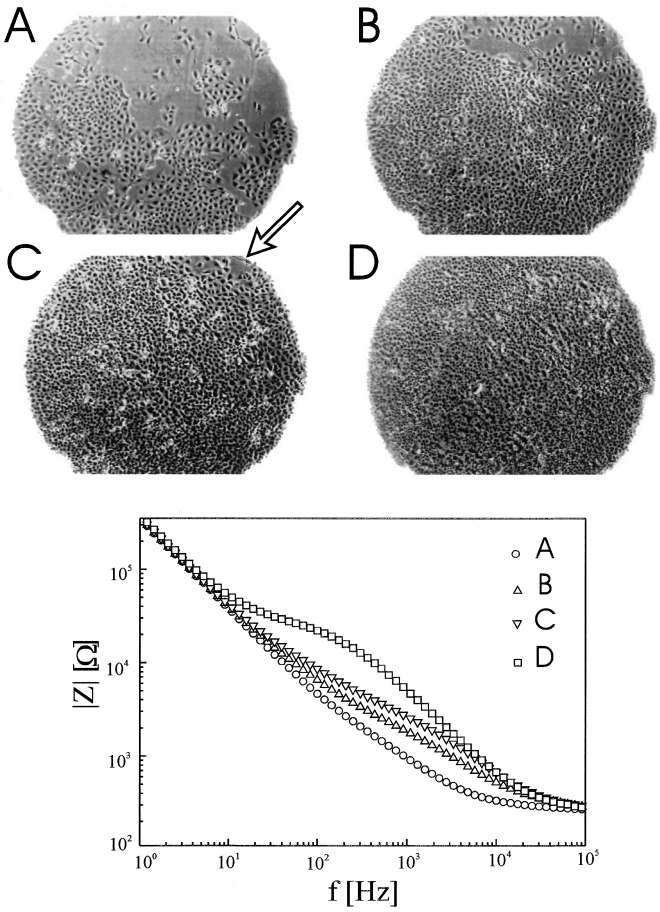

Fig. 4 Correlation between electrode coverage measured by impedance spectroscopy and visualized by phase-contrast-microscopy. It is remarkable that a detectable transepithelial resistance $R_{c.l.}$ appears only if complete coverages with confluent cells are achieved. This fact suggests the use of the *cell mode* measurement for an unambiguous detection of confluent cell monolayers with complete and reproducible electrode coverage. Because the quartz-crystal is almost opaque, owing to the gold electrodes evaporated on both sides, we used a reference-chamber consisting of transparent gold electrodes

be in good aggreement with published data for the same cell types, indicating that the shear vibration of the quartz plate does not alter epithelial barrier function.

Figure 4 is intended to illustrate the sensitivity of *cell mode* measurements in determining defects within the cell monolayer on top of the quartz electrode. Phase contrast micrographs in Fig. 4 A to 4 D show MDCK-II cells on top of gold electrodes (compare 2.3) in different culture stages, together with the corresponding *cell mode* impedance spectra. Obviously, the characteristic impedance spectrum of the cell covered gold electrode as shown in Fig. 2 B is only achieved if the gold electrode is entirely covered with a confluent epithelial cell monolayer. Small areas of uncovered electrode surface (note the arrowhead in Fig. 4 C) are sufficient to completely change the appearance of the *cell mode* spectrum and to hinder a meaningful quantitative analysis with the given equivalent circuit.

3.2 Quartz mode measurements

Figure 5 presents typical phase spectra ($\Phi(\nu)$) of the quartz resonator close to its resonance frequency of about 5 MHz (first harmonic) before and after removal of a confluent MDCK-I cell-monolayer. The appearance of the corresponding spectra for MDCK-II cell monolayers (data not shown) is very similar to those shown in Fig. 5 for MDCK-I cells. The parameters, resulting from quantitative analysis of the spectra, differ according to the individual properties of either cell type as discussed below.

As the phase angle spectrum of a quartz resonator may be regarded as analogous to any resonance curve, it is obvious without quantitative analysis that the shear vibration of the quartz plate is strongly damped by the presence of MDCK-I and MDCK-II cell monolayers. The decreased phase angle maximum, as well as the broadening of those spectra, for cell covered quartz resonators compared to uncovered resonators is a direct hint for the cellular damping of the shear displacement.

Quantitative information may be provided by fitting the parameters of the equivalent circuit shown in Fig. 3 B to the experimental data. This equivalent circuit simulates the electrical characteristics of the shear resonator over a range of frequencies close to the resonance region. Owing to the piezoelectric coupling between mechanical displacement and electrical potential of the quartz resonator, the parameters of the equivalent circuit should be related to the mechanical properties of the resonator and its loading. Martin et al. (1991) and Muramatsu et al. (1988) presented two different models for Newtonian liquids in contact with a quartz surface, both of which allow one to express the pa-

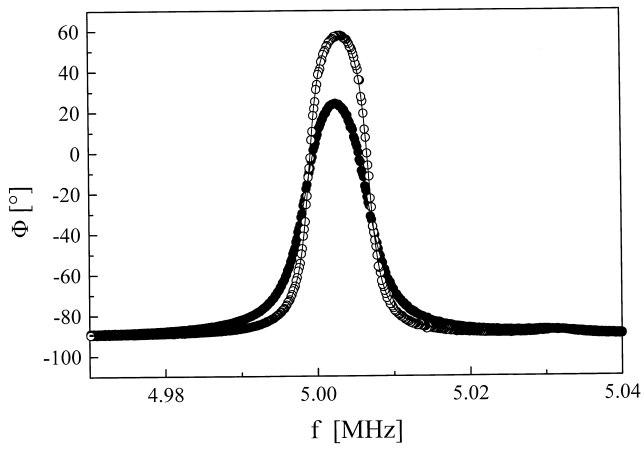

Fig. 5 Typical *quartz mode* phase spectra [Φ (f)] of the quartz resonator before (●) and after (○) removal of a confluent MDCK-I cell monolayer. The corresponding non-linear-least-square fit using the equivalent circuit depicted in Fig. 3B is given as the *solid line*. Before removal of the MDCK-I cell layer: $L_{total} = 46.8262$ mH, $R_{total} = 1487\ \Omega$, $C_P = 6.954$ pF. After removal: $L_{total} = 46.8188$ mH, $R_{total} = 673\ \Omega$, $C_p = 6.974$ pF

rameters of the given equivalent circuit in terms of physical properties of the quartz plate and those of the contacting liquids. Whereas Muramatsu et al. limited the influence of liquid loading to the motional resistance R, Martin et al. have also considered its influence on the motional inductance L. These authors extended their theoretical deduction to the treatment of simultaneous mass and liquid loading. As far as the motional resistance R is concerned both models uniformly predict R to be proportional to the square root of the density-viscosity-product of the contacting liquid. Therefore we have analyzed and discussed our experimental data for epithelial cell monolayers with respect to Martin's model.

Martin's theory is based on several assumptions necessary to keep the model on a simplified level. Beside the assumption of a continuous shear wave across the solid-liquid interface (nonslip condition), the velocity field within the liquid was modeled by solving the one dimensional Navier-Stokes equation for Newtonian liquids which provides the linkage to the physical properties of the contacting liquids in terms of their viscosity η and their density ρ. The following equations (1)–(6) summarize the predictions from Martin's theoretical approach to express equivalent circuit parameters with the physical properties of the quartz plate and those of mass and liquid loading.

The parallel capacitance C_P dominates the impedance characteristics of the quartz resonator in frequency ranges away from resonance. C_p has to be regarded as the sum of the capacitance C_0, that describes the quartz plate as a simple plate capacitor with the quartz material regarded as the dielectric filling, and the stray capacitance C_s arising from the connecting cables and the crystal holder. We did not determine the capacitances C_0 and C_s separately, but only the sum of both, C_p. The static capacitance C_0 may be expressed by Eq. (1):

$$C_0 = \varepsilon_{22} \frac{A}{d} \tag{1}$$

where ε_{22} denotes the dielectric permittivity of AT-cut quartz ($\varepsilon_{22} = 4.0221 \cdot 10^{-11}\ C^2J^{-1}\ m^{-1}$), A the surface area of the quartz electrode ($A = 0.27\ cm^2$) and d the thickness of the quartz plate. The parameters C, L, and R describe the motional branch for the unperturbed quartz resonator which dominate the impedance characteristics near resonance:

$$C = \frac{8 K_p^2 C_0}{(N\pi)^2} \tag{2}$$

$$L = \frac{1}{\omega_s^2 C} \tag{3}$$

$$R = \frac{\eta_q}{\bar{c}_{66} C} \left(\frac{\omega}{\omega_s} \right)^2 \tag{4}$$

Herein K_P denotes the cut-dependent electromechanical coupling constant of quartz ($K_P = 8.8876 \cdot 10^{-2}$ for an AT-cut quartz-crystal), N represents the overtone or harmonic number of the shear displacement (exclusively N = 1 in the present study), ω_s is the series resonant angular frequency of the quartz plate, η_q is the viscosity of the quartz crystal and $\bar{c}_{66}$ its "piezoelectrically stiffened" elastic constant.

Liquid as well as mass loading of the quartz resonator create additional impedance elements such as R_{load} and L_{load} that according to Martin et al. (1991) may be expressed as given in Eqs. (5) and (6).

$$R_{load} = \frac{\omega_s L}{N\pi} \sqrt{\frac{2\omega\rho\eta}{\bar{c}_{66}\rho_q}} \tag{5}$$

$$L_{load} = \frac{2\omega_s L \rho_s}{N\pi\sqrt{\bar{c}_{66}\rho_q}} + \frac{\omega_s L}{N\pi} \sqrt{\frac{2\rho\eta}{\omega\rho_q\bar{c}_{66}}} \tag{6}$$

where η_q and ρ_q denote the viscosity and the density of the quartz crystal, η and ρ represent the viscosity and density of the contacting liquid and ρ_s is the density of the surface attached mass layer. Equations (4), (5) and (6) demonstrate that R, R_{load} and L_{load} are dependent on the angular frequency ω. But as these circuit elements only contribute significantly to the total impedance of the quartz resonator in close proximity to the resonance region, one is justified in treating these elements as frequency independent, replacing ω by ω_s ($\omega = \omega_s$). Compared to a mechanical analogue, R_{load} may be regarded as the power dissipation due to the propagation of a damped shear wave into the liquid contacting the oscillating QCM-surface. R_{load} is therefore markedly influenced by the density and viscosity of the liquid loading. L_{load} represents changes of the QCM stored energy as a rigid mass layer on top of the quartz surface as well as an entrained liquid layer which move synchronously with the resonator surface, both regarded as additional masses, increase its kinetic energy. The first term of Eq. (6) represents the contribution of the surface attached mass layer whereas the second term is attributed to the liquid loading.

Although Fig. 3 B implies – for the sake of clarity – that the parameters of the unperturbed quartz (L, R) and those due to its loading (R_{load}, L_{load}) may be determined separately, this is experimentally not the case. The fitting routine only provides the total values of these impedance elements (R_{total}, L_{total}) for the loaded quartz resonator.

$$R_{total} = R + R_{load} \quad (7)$$

$$L_{total} = L + L_{load} \quad (8)$$

For reasons discussed elsewhere (Noël and Topart 1994) it is reasonable to fix the motional capacitance C to a constant value as it is only dependent on the physical properties of the quartz resonator but not on those of the loading. Some problems arise when determining the correct value for the capacitance C (Fig. 3 B). In order to find an appropriate value for the unperturbed as well as the loaded resonator, we followed the considerations of Noël and Topat (1994), who used the combination of Eqs. (1) and (2) to determine the capacitance C. The only missing parameter in Eq. (1) is the thickness d of the quartz crystal. The value of d can be calculated from the resonance frequency f_s of the quartz operating in air.

$$d = \frac{K_r}{f_s}, \quad (9)$$

where K_r denotes the cut related quartz resonance constant ($K_r = 1664\ s^{-1} \cdot m$ for AT-cut) and f_s the series resonance of the quartz in air. Combining Eqs. (1), (2) and (9) leads to the following expression for the motional capacitance C (N = 1):

$$C = \frac{8 K_p^2 A \varepsilon_{22}}{\pi^2 K_r} f_s \quad (10)$$

In our experiments C amounts to 21.655 fF as an average value. This value was taken as a constant in each experiment.

The outcome of the fitting routine in a typical experiment is given in Fig. 5 for a confluent MDCK-I cell monolayer before and after its detachment (solid line). The resulting parameters are given in the corresponding figure captions. Table 1 summarizes the mean results (±SDM) as they were determined in eight independent experiments (n = 8) for MDCK-I cell monolayers and seven independent experiments (n = 7) for MDCK-II cell layers.

Whereas the parameter R_{total} is roughly the same for the different quartz dishes after cell removal with only little scattering, the absolute value L_{total} is quite different for the various quartz dishes owing to differences of the quartzes themselves. Therefore, statistical treatment of this parameter for the various experiments is only reasonable using the differences ΔL_{total} between the cell covered quartz resonator and the quartz solely immersed in culture medium. Obviously the presence of surface attached MDCK-I and MDCK-II cell monolayers provides a significant increase of the parameters R_{total} as well as L_{total} of the quartz resonator, reflecting a strong damping of the quartz shear displacement and an increased stored energy. With respect to both parameters R_{total} and L_{total} MDCK-II cell layers

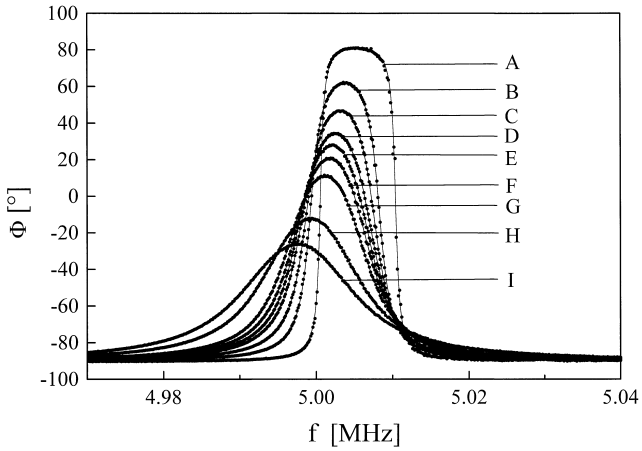

Fig. 6 Phase spectra (points) of the quartz crystal in the presence of different water-glycerol mixtures. The phase maximum decreases and the resonance curve broadens with increasing amounts of glycerol. (*A*) air, (*B*) water, (*C*) 40% glycerol, (*D*) 55% glycerol, (*E*) 60% glycerol, (*F*) 65% glycerol, (*G*) 70% glycerol, (*H*) 80% glycerol, (*I*) 85% glycerol. The *solid lines* represent the fitting curves according to the equivalent circuit shown in Fig. 3 B

($\Delta R_{total} = 992 \pm 36\ \Omega$, $\Delta L_{total} = 10.5 \pm 0.8\ \mu H$) exhibit a significantly stronger influence on the quartz shear vibration than MDCK-I cells ($\Delta R_{total} = (755 \pm 36)\ \Omega$, $\Delta L_{total} = (6.7 \pm 0.7)\ \mu H$). The influence of the culture medium on the parameters R_{total} and L_{total} may be omitted for the cell covered quartz resonator as the cell monolayer covers the electrode completely, which is confirmed by *cell mode* measurements, and the transverse shear wave is damped down in cellular dimensions. The cellular parameters $R_{c.l.}$ and $C_{c.l.}$ are in the same range as described elsewhere, indicating the completeness of the cell layer and the intactness of cell-cell-contacts.

In order to express the properties of the cell layers in the QCM experiments in terms of densities and viscosities we chose to calibrate our experimental setup by the use of different water/glycerol mixtures of known densities and viscosities. Figure 6 shows the phase-spectra for the different calibration liquids that were analyzed with the given equivalent circuit (Fig. 3 B). According to Eqs. (4) and (5) it seems reasonable to use the parameter R_{total} for the calibration procedure as this parameter is affected only by the physical properties of the quartz plate itself and the viscous properties of the liquids. However, it is incorrect to use L_{total} for the calibration experiment, as this parameter is additionally determined by the rigid mass loading which is supposed to be different for the water/glycerol system compared to the immobilized cell monolayers.

To avoid any errors arising from changes in R due to differences within different quartz plates or the glueing of the glass top, we used exactly the same quartz dishes for calibration measurements that were used to investigate the cell layers' properties as given in Table 1. Figure 7 A depicts the parameter R_{total} plotted against the square-root of the density-viscosity-product of different glycerol/water-mixtures together with the corresponding linear regression. The excellent correlation (r = 0.9997) for the entire viscos-

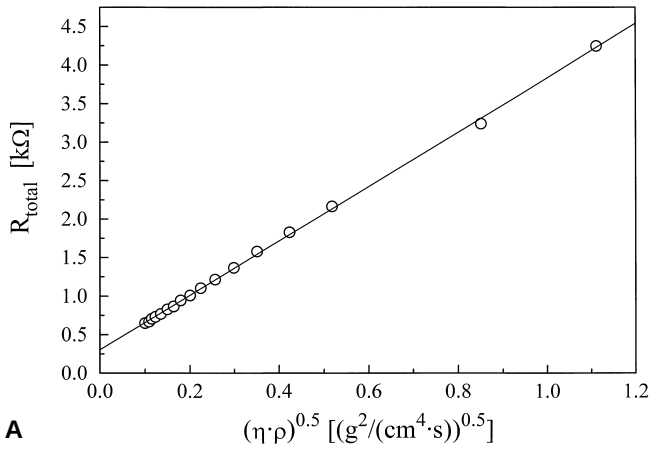

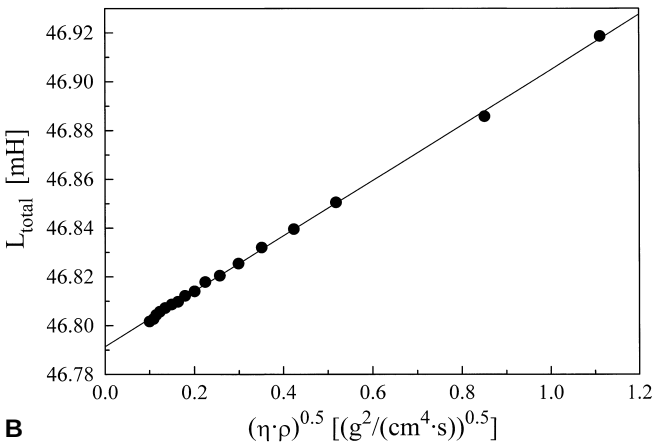

Fig. 7 **A** The dependence of the motional resistance $R_{total,}$ obtained from fitting the phase spectra of the different water/glycerol mixtures shown in Fig. 6, on the density-viscosity-product is demonstrated. The *solid line* represents the linear regression according to Eq. (11). The obtained parameters are: $A_R = (3531\pm22)$ $\Omega/(g^2/(cm^4s))^{0.5}$, $B_R = (304\pm9)$ Ω. **B** The inductance L_{total} is plotted versus the density-viscosity-product. The solid line represents the linear regression according to Eq. (13). $A_L = (112.2\pm0.9)$ μH/$(g^2/cm^4s))^{0.5}$, $B_L = (46.79\pm0.01)$ mH

ity range confirms the prediction of Martin's theory, that may be expressed by Eq. (11) after simple rearrangement of Eqs. (4), (5) and (7).

$$R_{total} = A_R\sqrt{\eta\rho} + B_R. \quad (11)$$

Using the parameters A_r and B_r provided by the linear regression together with the particular value for R_{total} we were able to calculate the apparent density-viscosity-product of either cell monolayer. Results are summarized in Table 2. As cellular densities were estimated by Percoll-centrifugation, we could use the density-viscosity-product to calculate the apparent viscosity of the cell monolayers. Cellular densities and apparent viscosities are detailed in Table 2. As already indicated by the differences of the motional resistances R_{total} for the two different cell types, MDCK-I and MDCK-II cell monolayers exhibit slightly

Table 2 Apparent viscosities η_{app} of MDCK-cell monolayers as derived from the motional resistance of the shear resonator R_{total} covered with the particular cell type (Table 1) and its calibration via known glycerol/water-mixtures as shown in Fig. 7 A. The cellular densities necessary to calculate η_{app} from the viscosity-density-products were obtained from Percoll-centrifugations. The slightly different densities ρ of the two cell types do obviously not account for the significantly different viscosity-density-products

	R_{total} [Ω]	$(\eta\cdot\rho)^{0.5}$ $[(g^2/(cm^4s))^{0.5}]$	ρ [g/cm^3]	η_{app} [g/(cm · s)]
MDCK I	1444±28	0.320±0.009	1.053±0.005	0.097±0.006
MDCK II	1673±22	0.386±0.008	1.051±0.005	0.142±0.006
Medium	686±8	0.103±0.005	1.004±0.005	0.011±0.003

different apparent viscosities. According to Eqs. (3), (6) and (8) the total inductance of the quartz resonator is determined by the physical properties of the quartz resonator itself as well as mass and liquid loading. As any of these contributions provides an additional term to the total inductance, we tried to distinguish between the contribution of surface attached rigid mass and liquid loading. In order to quantify the influence of viscous liquid loading on the motional inductance, it is reasonable to combine Eqs. (6) and (8) to yield Eq. (12):

$$L_{total} = L + L_{mass} + L_{\eta\rho} \quad (12)$$

With respect to the influence of the density-viscosity-product of the contacting liquid Eq. (12) may be expressed as

$$L_{total} = A_L\sqrt{\eta\rho} + B_L. \quad (13)$$

Herein the contributions of L and L_{mass} are taken together in the parameter B_L, which may be different in our cellular system compared to the calibration system. However, the parameter A_L may be regarded as a constant that allows one to calculate the inductance contribution due to the density-viscosity-product of the contacting liquid. In Fig. 7 B the total inductance L_{total} of the glycerol/water mixtures is plotted against the square root of their density-viscosity-products together with the corresponding linear regression. Even here the linear relationship between L_{total} and $(\eta\cdot\rho)^{0.5}$ – as predicted by Martin et al. – is confirmed for the entire abscissa range ($r = 0.9996$). Using the parameter A_L as deduced from the linear regression together with the apparent density-viscosity-products of the two cell types and the culture medium (Table 2) we can calculate the inductance contribution $L_{\eta\rho}$ due to the viscous properties of either system. Results are summarized in Table 3. The increase of $L_{\eta\rho}$ caused by the presence of either cell monolayer relative to the culture medium is given as $\Delta L_{\eta\rho}$. Surprisingly $\Delta L_{\eta\rho}$ as calculated by the assumption of Martin's model is larger than experimental changes of the total inductance ΔL_{total} for both cell monolayers with respect to the pure culture medium. Calculation of a surface attached mass for the cell covered quartz resonator is therefore impossible as it would require $\Delta L_{\eta\rho}$ to be smaller than ΔL_{total} so that the difference between both parameters could be attributed to rigid mass loading.

Table 3 Assuming Martin's model for Newtonian liquids, liquid loading of the shear resonator causes the motional inductance to shift owing to entrained liquid layers. The amount of shifting is dependent on the viscosity-density-product of the particular liquid (Eq. (6)). Here $L_{\eta\rho}$ represents the calculated shift of the motional inductance arising from the viscous properties of the cell monolayers or the culture medium, respectively, based on Eqs. (12) and (13) using the viscosity-density-products of the cell layers and the medium as given in Table 2. $\Delta L_{\eta\rho}$ stands for the calculated shift of the motional inductance caused by the cell monolayers relative to pure culture medium. In opposition to these calculated changes of the motional inductance, ΔL_{total} presents the experimentally observed total changes of the motional inductances with respect to the culture medium. ΔL_{total} being greater than $\Delta L_{\eta\rho}$ could be easily explained by an additional surface mass deposition, which is known to influence L_{total}, but our findings call for a different interpretation which is discussed below (p. d. per definitionem)

	$L_{\eta\rho}$ [μH]	$\Delta L_{\eta\rho}$ [μH]	ΔL_{total} [μH]
MDCK-I	35.9	24.3	6.7
MDCK-II	43.3	31.7	10.5
Medium	11.6	0 (p. d.)	0 (p. d.)

Possible explanations for our findings are discussed in the following section.

4. Discussion

The present study introduces a new technique to analyze different properties of confluent epithelial cell-monolayers grown on shear wave resonators. Two different impedance spectroscopic experiments were combined to determine either the transepithelial resistance $R_{c.l.}$ of the cell-layers together with their capacitances $C_{c.l.}$ (*cell mode*) or their viscoelastic properties as extractable from the cell-layers' influence on the shear vibration of the quartz resonator (*quartz mode*).

4.1 Cell mode measurements

Cell mode measurements as presented in Fig. 2 A for the tight epithelial MDCK-I and in Fig. 2 B for the leaky epithelial MDCK-II, respectively, allow one to document the intactness of confluent cell monolayers grown on the gold-electrodes of the quartz resonator. Fitting the impedance spectra with the equivalent circuit shown in Fig. 3 A provides two independent parameters of the cell-monolayers, the transepithelial resistance $R_{c.l.}$ and its capacitance $C_{c.l.}$ (Table 1), suitable to indicate defects within electrode coverage or cell-cell-contacts. In this study we mainly used this method, recently described in detail (Wegener et al. 1996), to confirm complete electrode coverage and intactness of the confluent cell-layer before and after the experiments in the *quartz mode* as an unconditional prerequisite for a reasonable determination of the apparent viscosity. The suitability of this method to detect even small amounts of defects in the cell-monolayer was confirmed by the photocorrelation experiment demonstrated in Fig. 4. We used the *cell mode* measurement since common microscopic methods such as phase contrast microscopy fail to determine the completeness of the cell-monolayer due to the almost opaque gold electrodes on both sides of the quartz-crystal. Furthermore, impedance analysis in the *cell mode* has the advantage of being performable at any time within a QCM experiment just by using the computer controlled relay to change the measuring mode, and therefore avoiding any manipulation of the quartz resonator. Another very important aspect in this context is the ability of *cell mode* measurements to show that the continuous shear stress arising from the shear oscillation of the resonator does not damage the adherent cells. The cell layers remained unaffected by the applied shear stress as far as their passive electrical properties and their viscous-properties are concerned. The principal reason for this could be the reduced displacement-amplitude of the shear wave reaching the cell-layer as it is well known that adherent cells establish a considerable gap between their ventral surface and the substrate, which is supposed to be filled with proteins of the extracellular matrix. Martin and Hager (1988) roughly estimated the amplitude of oscillation in water to about 1 – 2 nm, which is small compared to the lateral dimensions of the cells ($8\times8\times10\ \mu m^3$) (Richardson et al. 1981).

4.2 Quartz mode measurements

The most important result of this study is to confirm that cells immobilized on a quartz surface increase the damping of the resonator's shear displacement due to their viscoelastic properties, similar to the behavior of liquids in contact with the quartz plate. This fact can be easily deduced from the appearance of the phase spectra shown in Fig. 5, in which the attached cell-monolayers cause a broadening of the peak (decrease in $|d\Phi/df|$) and a decrease in the phase maximum as well as a small translation to lower frequencies. Previously, different studies provided some indirect hints that the influence of adherent cell-layers on the shear displacement is predominantly of damping nature (Redepenning et al. 1993; Ebato et al. 1993; Gryte et al. 1993), but no quantification was possible so far. Network analysis of impedance data recorded in *quartz-mode* measurements allows one to quantify cellular damping properties. The resistance R_{total} representing the sum of all damping contributions increases dramatically when cells are in contact with the quartz surface, providing apparent cell viscosities up to $0.097\ g\cdot(cm\cdot s)^{-1}$ for MDCK-I and $0.142\ g\cdot(cm\cdot s)^{-1}$ for MDCK-II cells based on the calibration experiment with different water/glycerol mixtures as described in the result-section. A very interesting observation in this context was the fact that the translation of the phase spectra to lower frequencies, equivalent to an increase in L_{total}, was not as marked as expected from the corresponding water/glycerol mixture (Fig. 6) which possesses the same apparent density-viscosity product. Following Martin's theory for Newtonian liquids in contact with the quartz surface both L_{total} and R_{total} exhibit a linear dependence on the square root of the density-vis-

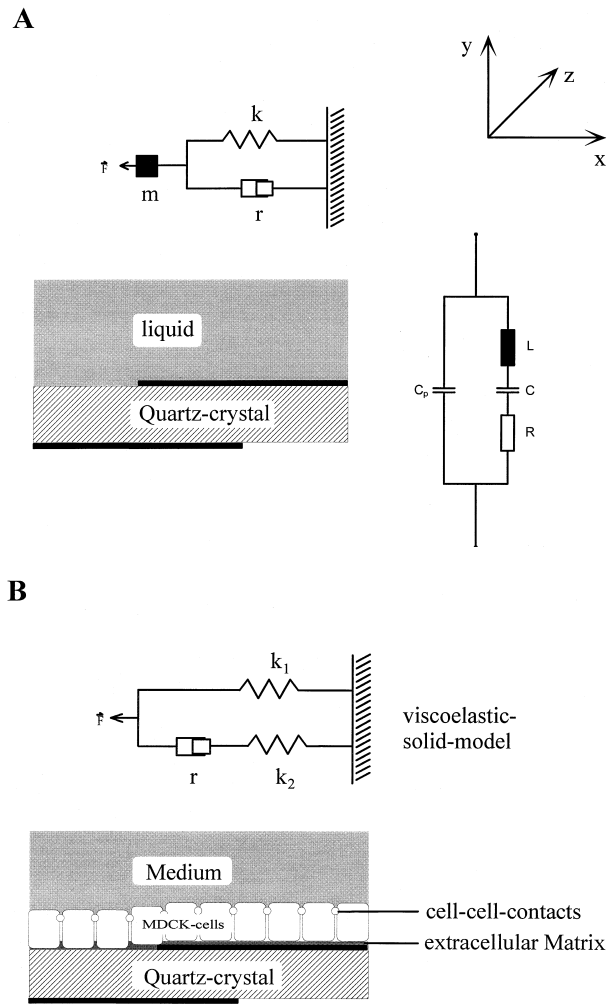

Fig. 8 **A** Mechanical and electrical model of an AT-cut quartz resonator according to Muramatsu et al. (1988). **B** Schematic view of the attached cell-monolayer on the quartz plate. The viscoelastic solid-model representing the cell-monolayer is shown. For detailed information see text

cosity-product of the loaded liquid as expressed in Eqs. (5)–(6). Inserting the density-viscosity-products of the cell-layers (derived from the calibration of the motional resistances R_{total}) into Eq. (13) for the inductance L_{total}, in order to determine the inductance contribution due to mass-loading, gave negative values. These findings indicate that Martin's model derived for semi-infinite Newtonian-liquids in contact with the resonator's surface is too simplified to account for the viscoelastic properties of an immobilized cell-monolayer. Different rheological models have been developed to describe the short time, small deformation response of granulocytes to applied forces (Evans and Yeung 1989; Tran-Son-Tay et al. 1991). Considering the most basic of them, the viscoelastic-solid model (Fig. 8), the cell is treated as a standard elastic solid with an elastic element k_1 in parallel with a Maxwell element consisting of a spring k_2 in series with a viscous element r. These additional elastic components, respresented by k_1 and k_2, could be the explanation for the deviations we found for the inductance L_{total}. Owing to the fact that the inductance L and the capacitance C, as given in the equivalent circuit of Fig. 3B, are indistinguishable by fitting the impedance data, because L and C are strongly correlated (the greater L, the smaller C and vice versa), it seems to be reasonable that an additional capacitance C_{load}, due to new elastic elements could produce a smaller increase in L than expected. This interpretation is based on the analogy between a capacitance in the electrical system and an elastic constant in its mechanical equivalent (Muramtsu et al. 1988). It should be emphasized that alteration of C by elastic material on the quartz surface was not mentioned before. This possible L-compensating effect due to the elastic properties of the cell-monolayer remains to be elucidated in future experiments. In this context it is very important to mention the work of Reed et al. (1990), who describe an AT-cut quartz resonator loaded with viscoelastic material. They discussed the role of an elastic medium with viscous losses in terms of a complex elasticity or viscosity, respectively. Particularly the discrepancy in the measured viscosities for polymers with high molecular weight could be explained by assuming a complex, frequency dependent viscosity.

Another interesting feature within the cellular viscous properties is the influence of the different cell-cell-contacts between adjacent cells. It is well known that adherence junctions and desmosomes provide a linkage between the actin and keratin cytoskeletons of neighbouring cells which is predominantly responsible for the mechanical stability of a cell-monolayer. Another aspect, not yet investigated, arises from the assumed gap between the cell-monolayer and the quartz surface filled with a considerable amount of extracellular matrix as mentioned above. This could cause a significant spacing between the cell and the substrate bringing about an additional interface with unknown viscosity. Assuming that the viscosity of the layer between cells and substrate possesses a lower apparent viscosity than the adherent cells the shear wave could be considerably damped down before entering the cell-monolayer. This may cause a systematic error towards underestimating the apparent viscosities of the MDCK-cells. Considering recently published work from Evans and Yeung (1989) much higher apparent viscosities ($2000\ g \cdot (cm \cdot s)^{-1}$) for granulocytes were measured by the micropipette-method.

With respect to the energetic interpretation of the Butterwoth-Van-Dyke equivalent circuit, the motional inductance L_{total} represents the energy storage of the shear resonator, which is determined by the kinetic energy of the oscillating mass, including rigid mass loading and entrained liquid layers. The motional resistance, however, reflects energy losses due to the propagation of the shear wave into a viscous liquid. In the case of liquid loading, any entrained liquid layer and the damping bulk are substantially identical. In the cellular system only the proteins, providing anchoring of the cells to the surface, are in direct contact with the resonator's surface, whereas the cellular body – responsible for the high damping – is only

more or less close to the quartz-plate. Therefore it seems reasonable to expect that the presence of the cell-layer is much more pronounced in the parameter R than in L.

Assuming those very high viscosities, as described for granulocytes, for the attached cell-monolayer another explanation may account for the underestimation of the viscosities measured with our method. As higher viscosities increase the decay length δ of the shear wave according to Eq. (14):

$$\delta = \sqrt{\frac{2\eta}{\rho\omega}}, \tag{14}$$

the decay length may surpass the mean thickness of the cell-monolayer leading to a decreased apparent viscosity. As the medium on top of the cell-layer exhibits much lower viscous damping (Table 1) than the cell-layer itself, only a mean value for this two phase system should be obtainable. To exclude this possible source of error we performed an additional experiment in which we loaded the confluent cell-monolayer with silicon beads, while recording simultaneously the resonant frequency of the quartz-plate (data not yet published). No decrease in frequency could be observed, neither with impedance analysis nor with the active oscillator method. This result clearly confirms that the shear wave does not escape from the cell-monolayer with a significant amplitude.

Though many problems remain to be elucidated, impedance spectroscopy applied in the case of confluent epithelial cell-monolayers cultured on quartz crystals offers new insights into the viscoelastic behavior of cells under certain conditions. Furthermore, impedance analysis has several advantages compared to the commonly used active oscillator-method. In contrast to the oscillator-method, the network analysis can distinguish the parameter R representing damping from the inductance L mainly indicating mass-load. Detection of the series resonant frequency only, using common oscillator devices, in order to investigate the viscous properties of cell-layers must be handeled with extreme care as the inability to resolve the parameters R and L could give rise to misinterpretations. As revealed in this study the attached cells could change L and R in a non liquid like manner. The density-viscosity-product determined by using Kanazawa-Gordon's equation (Kanazawa and Gordon 1985) for the series-resonance frequency under liquid loading will be different to those obtained by impedance analysis.

Another remarkable point is the fact that very high viscosities, which create phase maxima below zero degrees, cannot be detected using the active oscillator method because this technique is limited to positive phase maxima. Impedance spectroscopy, however, can be used even at negative phase maxima and is therefore more suitable for higher viscosities.

Acknowledgements The authors are very much indepted to Dipl.-Ing. W. Willenbrinck and Dipl. Ing. W. Wilting for their expert help with all kinds of electronic problems. This work was supported by the German ministry of education and research (BMBF), grant number 310 855. Joachim Wegener is recipient of a grant from the Studienstiftung des Deutschen Volkes, Andreas Janshoff was supported by a scholarship granted by the Fonds der Chemischen Industrie. We would like to thank Dipl.-Chem. C. Steinem and D. Trommeshauser for helpful discussions.

References

Ebato H, Okahata Y, Matsuda T (1993) Detection of cell adhesion behaviors by using a quartz crystal microbalance. Kobunshi Ronbunshi 50: 463–469

Evans E, Yeung A (1989) Apparent viscosity and cortical tension of blood granulocytes determined by micropipet aspiration. Biophys J 56: 151–160

Glassford AMP (1978) Response of a quartz crystal microbalance to a liquid deposit. J Vac Sci Technol 15: 1836–1843

Gryte DM, Ward MD, Hu WS (1993) Real-time measurement of anchorage dependent cell adhesion using a quartz crystal microbalance. Biotechnol Prog 9: 105–108

Kanazawa KK, Gordon JG (1985) Frequency of a quartz microbalance in contact with liquid. Anal Chem 57: 1770–1771

Kippling AL, Thompson M (1990) Network analysis method applied to liquid-phase-acoustic wave sensors. Anal Chem 62: 1514–1519

McAdams ET (1995) The linear and non-linear electrical properties of the electrode-electrolyte interface. In: Gersing E, Schaefer M (eds) Proceedings of the IX International Conference on Electrical Bio-Impedance, pp 5–8

Martin BA, Hager HE (1988) Velocity profile on quartz crystals oscillating in liquids. J Appl Phys 65: 2630–2635

Martin SJ, Granstaff VE, Frye GC (1991) Characterization of a quartz crystal microbalance with simultaneous mass and liquid loading. Anal Chem 63: 2272–2281

Muramatsu H, Dicks JM, Tamiya E, Karube I (1987) Piezoelectric crystal biosensor modifield with protein A for determination of immunoglobulins. Anal Chem 59: 2760–2763

Muramatsu H, Tamiya E, Karube I (1988) Computation of equivalent circuit parameters of quartz crystals in contact with liquids and study of liquid properties. Anal Chem 60: 2142–2146

Noël AM, Topart PA (1994) High-frequency impedance analysis of quartz crystal microbalances. 1. General considerations. Anal Chem 66: 484–491

Reed CE, Kanazawa KK, Kaufman JH (1990) Physical description of a viscoelastically loaded AT-cut quartz resonator. J Appl Phys 68: 1993–2001

Redepenning J, Schlesinger TK, Mechalke EJ, Puleo DA, Bizios R (1993) Osteoblast attachment monitored with a quartz crystal microbalance. Anal Chem 65: 3378–3381

Richardson JCW, Scalera V, Simmons VL (1981) Identification of two strains of MDCK cells which resemble separate nephron tuble segments. Biochim Biophys Acta 673: 26–36

Sauerbrey G (1959) Verwendung von Schwingquarzen zur Wägung dünner Schichten und zur Mikrowägung. Z Phys 155: 206–222

Schneider TW, Buttry DA (1993) Electrochemical quartz crystal microbalance studies of adsorption and desorption of self-assembled monolayers of alkyl thiols on gold. J Am Chem Soc 115: 12 391–12 397

Tran-Son-Tay R, Needham D, Yeung A, Hochmuth RM (1991) Time-dependent recovery of passive neutrophils after large deformation. Biophys J 60: 856–866

Weast RC, Ed. (1984) Handbook of chemistry and physics. CRC Press, Bota Raton, FL

Wegener J, Sieber M, Galla HJ (1996) Impedance analysis of epithelial and endothelial cell monolayers cultured on gold surfaces. J Biochem Biophys Methods 32: 151–170

Xu H, Schlenoff JB (1995) Kinetics, isotherms, and competition in polymer adsorption using the quartz crystal microbalance. Langmuir 10: 241–245

Yang M, Thompson M (1993) Multiple chemical information from the thickness shear mode acoustic wave sensor in the liquid phase. Anal Chem 65: 1158–1168